



BRNO UNIVERSITY OF TECHNOLOGY

VYSOKÉ UČENÍ TECHNICKÉ V BRNĚ

FACULTY OF MECHANICAL ENGINEERING
FAKULTA STROJNÍHO INŽENÝRSTVÍ

INSTITUTE OF SOLID MECHANICS, MECHATRONICS AND BIOMECHANICS
ÚSTAV MECHANIKY TĚLES, MECHATRONIKY A BIOMECHANIKY

DESIGN AND IMPLEMENTATION OF ALGORITHMS FOR COMPENSATING THE EFFECT OF LINEAR ACCELERATION ON ANGULAR VELOCITY MEASUREMENTS BY MEMS GYROSCOPES

NÁVRH A IMPLEMENTACE ALGORITMŮ PRO KOMPENZACI VLIVU LINEÁRNÍHO ZRYCHLENÍ NA MĚŘENÍ ÚHLOVÉ RYCHLOSTI MEMS GYROSKOPY

SHORT VERSION OF DOCTORAL THESIS
ZKRÁCENÁ VERZE DOKTORSKÉ PRÁCE

AUTHOR
AUTOR PRÁCE

Ing. Tomáš Spáčil

SUPERVISOR
ŠKOLITEL

doc. Ing. Robert Grepl, Ph.D.

BRNO 2023

Keywords

MEMS sensors; gyroscope; accelerometer; feedforward compensator; mechatronics; Matlab; Simulink; FPGA; microcontroller; real-time calculations.

Klíčová slova

MEMS senzory; gyroskop; akcelerometr; dopředný kompenzátor; mechatronika; Matlab; Simulink; mikrokontrolér; výpočty v reálném čase.

Místo uložení rukopisu:

Knihovna VUT-FSI v Brně, Technická 2896/2, 616 69 Brno.

Tomáš Spáčil, 2023

ISBN 80-214-

ISSN 1213-4198

Contents

1	Introduction	4
2	Theoretical Survey	5
2.1	Inertia sensors	5
2.2	Model of MEMS gyroscopic sensor	6
3	Formulation of the thesis goals	7
3.1	Theoretical objective 1: Effects of linear acceleration and jerk on MEMS gyroscopic sensors and their quantification	7
3.2	Theoretical objective 2: Design of new models for linear acceleration compensation	7
3.3	Practical goal: Implementation of the proposed method on RT-HW and experimental measurements	8
4	Analysis of gyroscope measurement errors	9
4.1	Physical setup of the system	9
4.2	Observation A: cross-correlation between same gyroscopic sensors, random excitation	10
4.3	Observation B: cross-correlation between different gyroscopic sensors, random excitation	13
4.4	Observation C: different gyroscopic sensors, wide range of excitations	16
5	Compensational models	18
5.1	Non-Linear Least Squares	18
5.2	Artificial Neural Network - ANN	21
5.3	Summary	25
6	Implementation on RT HW	26
6.1	Artificial neural network algorithm	26
6.2	NLS-based compensator implementation and performance	27
6.3	Summary	29
7	Conclusion	30
7.1	Thesis achievements	30
7.2	Further research possibilities	31
	References	32

1 Introduction

Gyroscopes constitute a specialized class of devices designed to measure the angular velocity of a target object relative to a fixed reference frame. These instruments find applications across a diverse spectrum of human endeavors, ranging from underwater exploration to aerospace systems, and are integral not only to crewed missions but also to autonomous navigation and guidance systems. Essentially, gyroscopic sensors furnish critical data regarding an object's orientation or its rate of change in orientation, referred to as angular velocity.

MEMS (Micro-Electro-Mechanical Systems) gyroscopes operate on the principle of angular velocity measurement, from which orientation can be inferred by integration in time relative to an initial known state. Unique to this MEMS-based approach is its reliance on the Coriolis force which arises when there is a simultaneous presence of rotational and linear velocities along orthogonal axes. This force serves as the basis for deriving angular velocity measurements in MEMS gyroscopes.

In the context of MEMS gyroscopes, which are mass-based sensors, various complexities arise that can compromise the fidelity of measurements. These complexities are not confined solely to mechanical issues but extend to electrical considerations as well, as the inherent nature of MEMS fabrication is introduced. Within the scope of this research, our primary emphasis is placed on mechanical, respectively dynamical errors attributable to the fundamental force-mass interactions that govern the sensor's operation. This focus allows us to investigate the nontrivial relationship between dynamic forces and the resulting errors, providing an understanding that is crucial for developing effective compensatory algorithms.

2 Theoretical Survey

2.1 Inertia sensors

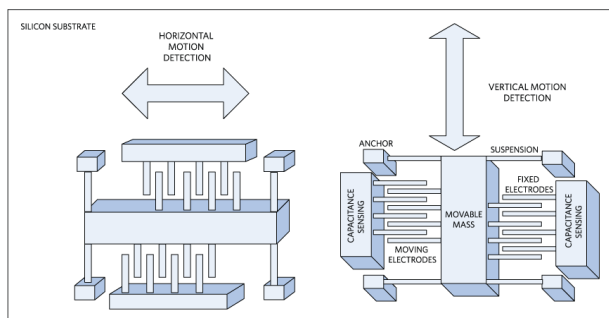


Figure 2.1: Accelerometer schematic. [1]

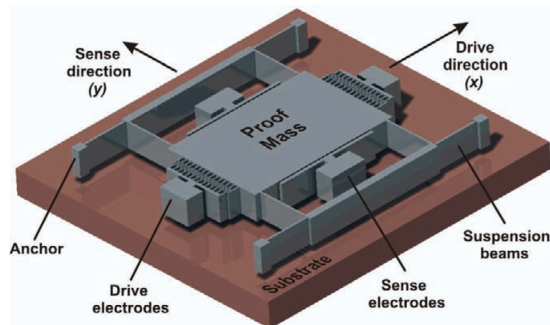


Figure 2.2: Gyroscope 3D model. [2]

Inertial sensors are key components in a broad range of systems, from consumer electronics and robotics to aerospace and automotive applications. These sensors provide critical information about an object’s movement and orientation within a physical space. Various types of inertial sensors exist, but we would point out two, elemental types, of them:

- **Accelerometers:** These sensors measure linear acceleration along one axis and potentially combined up to 3. They are extensively used in mobile devices for orientation detection, in automotive safety systems for airbag deployment, and in robotics for motion control. Their principle is based on the deflection of a spring and measurement of such a deflection, as can be seen in Figure 2.1.
- **Gyroscopes:** Gyroscopes measure the angular velocity, essentially the speed at which an object rotates around its axis. They find applications in various fields including aerospace for attitude control, automotive systems for stability, and in consumer electronics like smartphones for orientation and navigation. Their principle is not so straightforward as in the case of accelerometers, so we describe them further.

2.1.1 Design of gyroscopic sensors

Numerous designs of gyroscopic sensors exist, tailored for various key properties like precision, stability, price, or robustness. From a rich history, we point out here the MEMS gyroscopic sensor.

MEMS gyroscopes

To describe the mechanical part of the structure, we chose a simple gyroscopic sensor with a single oscillating mass (Proof Mass) in Figure 2.2.

In addition to the mechanical part, the MEMS gyroscope includes electronic elements such as voltage regulators, amplifiers, or filters. The principle of the function of the gyroscopic sensor is to transfer mechanical energy from one actively oscillating axis through the Coriolis force to the other, measuring axis. In the most common form, the active element consists of only one oscillating mass, but there are also gyroscopic sensors that have more oscillating masses.

2.2 Model of MEMS gyroscopic sensor

Oscillatory MEMS gyroscopic sensors operate based on a vibrating structure, usually a micro-scale mechanical resonator, as opposed to the spinning rotor found in traditional mechanical gyroscopes. The resonator is set into oscillation along a particular "drive" axis. When the sensor experiences an angular rotation about an axis orthogonal to the drive axis, the Coriolis effect comes into play, giving rise to the Coriolis force. The relation of coordinate systems in the scope of the problem and the origin of Coriolis force can be seen in Figure 2.3.

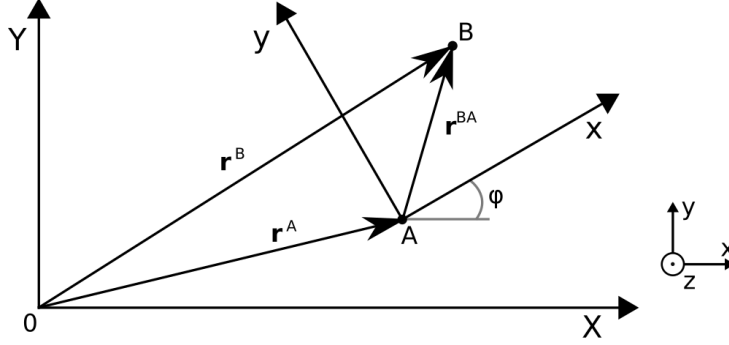


Figure 2.3: Substrate "A" vs. proof mass "B". [3]

$$\mathbf{r}^B = \mathbf{r}^A + \mathbf{r}^{BA} \quad (2.1)$$

$$\dot{\mathbf{r}}^B = \dot{\mathbf{r}}^A + \dot{\mathbf{r}}^{BA} + \dot{\boldsymbol{\varphi}} \times \mathbf{r}^{BA} \quad (2.2)$$

$$\ddot{\mathbf{r}}^B = \ddot{\mathbf{r}}^A + \ddot{\mathbf{r}}^{BA} + \dot{\boldsymbol{\varphi}} \times \dot{\mathbf{r}}^{BA} + \dot{\boldsymbol{\varphi}} \times (\dot{\boldsymbol{\varphi}} \times \mathbf{r}^{BA}) + \ddot{\boldsymbol{\varphi}} \times \mathbf{r}^{BA} + \dot{\boldsymbol{\varphi}} \times \dot{\mathbf{r}}^{BA} \quad (2.3)$$

$$\ddot{\mathbf{r}}^B = \ddot{\mathbf{r}}^A + \ddot{\mathbf{r}}^{BA} + \boldsymbol{\omega} \times (\boldsymbol{\omega} \times \mathbf{r}^{BA}) + \boldsymbol{\alpha} \times \mathbf{r}^{BA} + 2(\boldsymbol{\omega} \times \dot{\mathbf{r}}^{BA}) \quad (2.4)$$

$$m\ddot{x} + c_x\dot{x} + k_x x = F_{i,x} + F_{r,x} + m\omega_z^2 x + m\dot{\omega}_z y + 2m\omega_z \dot{y} \quad (2.5)$$

$$m\ddot{y} + c_y\dot{y} + k_y y = F_{i,y} + F_{r,y} + m\omega_z^2 y - m\dot{\omega}_z x - 2m\omega_z \dot{x} \quad (2.6)$$

where m is the weight of the seismic mass, c is the damping constant, k is the spring constant, F_i is the force acting on the seismic mass resulting from the movement of the rotating frame in the inertia frame, F_r is the force resulting from the electrostatic actuator, $m\omega^2 x$ ($m\omega^2 y$) is the term representing the centrifugal force, $m\omega \dot{x}$ ($m\omega \dot{y}$) is the term representing the Euler force, and $2m\omega \dot{x}$ ($2m\omega \dot{y}$) is the term representing the Coriolis force. These equations were derived in our previous work [3].

The formula for the Coriolis force is derived in 2.4 as following term 2.7.

$$\mathbf{F}_C = 2m(\boldsymbol{\omega} \times \dot{\mathbf{r}}^{BA}) \quad (2.7)$$

This force is then detected as a change in the amplitude or frequency of the oscillation along the sense axis. By measuring this change, the gyroscope can accurately determine the rate of angular rotation ω that caused the Coriolis force to be generated in the first place.

3 Formulation of the thesis goals

Currently, there are many fusion algorithms for estimating IMU rotation in space, but very little attention has been paid to parasitic effects acting on MEMS gyroscopes, which are an elementary part of the IMU. According to our study so far, we conclude that the linear acceleration, whose compensation is not entirely trivial and is often neglected, has a major influence on the measurements. This thesis will deal with the development of a new compensation algorithm that will be able to reduce the influence of linear acceleration on a MEMS gyroscopic sensor in real-time. We assume that this will subsequently lead to a more accurate fusion algorithm for estimating the rotation of the IMU unit in space. The individual objectives can be characterized as follows:

3.1 Theoretical objective 1: Effects of linear acceleration and jerk on MEMS gyroscopic sensors and their quantification

The effect of linear acceleration and jerk on MEMS gyroscopic sensors is a marginally investigated topic, but one that significantly affects sensor performance. Sensor manufacturers typically report sensitivity to constant linear acceleration, such as gravitational acceleration, in the form of a constant, which does not adequately capture the problem due to the complexity of the problem. Manufacturers very rarely report sensitivity to dynamic disturbance. The first objective of this dissertation will result in the definition of a unified procedure for quantifying the effect of linear acceleration and jerk on MEMS gyroscopic sensors. We will experimentally quantify the effect of linear acceleration and jerk on real sensors of different price categories.

3.2 Theoretical objective 2: Design of new models for linear acceleration compensation

A method will be proposed to compensate for linear acceleration using acceleration measurements and further processing. We assume that the compensation method will be generally nonlinear and the models used will be based on ANN, local linear models, or polynomial models.

If we compensate for the effect of linear acceleration before entering the fusion algorithm to estimate the rotation of the IMU unit in space, we will be able to estimate the rotation angle more accurately, or cheaper sensors can be used while maintaining the performance. Graphically, the resulting structure of the compensation algorithm can be defined as shown in Figure 3.1. The results from published papers [4] or [3] propose that the sensitivity to linear acceleration can be reduced considerably.

The output will be a mutual comparison of the robustness of several variants of our

3 FORMULATION OF THE THESIS GOALS

proposed approximators through simulations and experiments. We anticipate that the RCP approach on the dSPACE HW platform or NI PXI will be used for experimental testing of the algorithms.

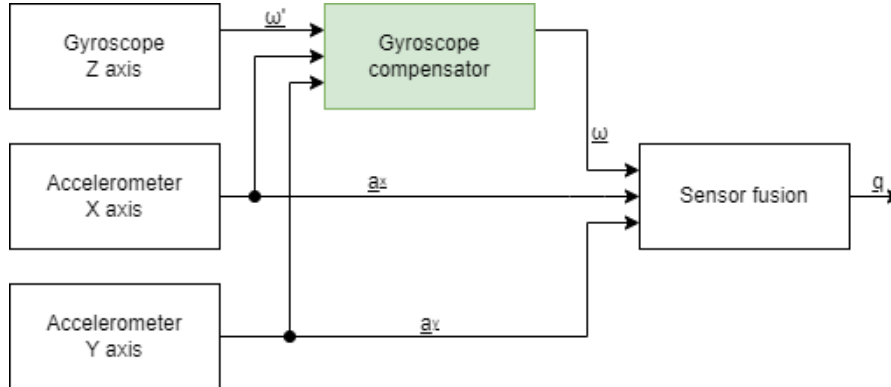


Figure 3.1: Compensator principle.

3.3 Practical goal: Implementation of the proposed method on RT-HW and experimental measurements

Based on the comparison of different algorithms in the previous objective, we will select a suitable compensation algorithm and implement it on a prototype Real-Time HW. It is suggested to use a microcontroller or an FPGA. We will evaluate the practicality of implementing the solution and determine the required HW. According to the resulting behavior in a real laboratory model, the contribution of the implemented compensator model will be quantified. A prototype control unit will be used, containing MEMS gyroscopes, accelerometers (IMUs), and a suitable processor, enabling signal processing by the newly proposed methods in real-time. In addition, a mechatronics measurement system will be constructed for measurement purposes and experiments will be performed on it. This system can then be used as a laboratory model for teaching intelligent machine control.

4 Analysis of gyroscope measurement errors

Motivated by our initial system of interest, the single axis two wheel unstable personal transporter, we constrained the frequency range under examination to a maximum of 10 Hz, a decision based on our observations that this range was most frequently relevant to the system’s performance. The subsequent chapters provide a standardized template for determining sensor sensitivity to linear acceleration, in support of theoretical objective 1.

4.1 Physical setup of the system

Since our work involves dealing with actual hardware, it was crucial to develop an appropriate testing environment and choose the right sensors for evaluation, with further details provided in this section.

4.1.1 Sensors selection and relative environment

In the interest of enhancing measurement accuracy, our experimental design incorporated a dual-measurement approach, wherein each test case was simultaneously run with its inverted, complementary sensor. The inherent advantage of this paired-measurement methodology lies in its potential for nullifying random measurement errors.

The subsequent sensors were chosen for evaluation.

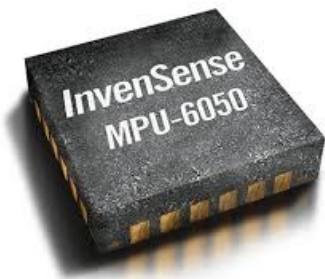


Figure 4.1: InvenSense MPU-6050. [5]



Figure 4.2: STMicroelectronics L3G4200D. [6]



Figure 4.3: Murata SCC2000. [7]

parameter	Gyroscope range	Acceleration range	Read-out frequency
value	$\pm 250 \text{ deg/s}$	$\pm 2 \text{ g}$	800 Hz

Table 4.1: InvenSense MPU-6050 custom settings.

Regarding the motor control strategy, we implemented direct current control with a sinusoidal waveform, which induces relative force directly on the gyroscope in a specified axis.

4 ANALYSIS OF GYROSCOPE MEASUREMENT ERRORS

parameter	Gyroscope range	Read-out frequency
value	$\pm 250 \text{ deg/s}$	800 Hz

Table 4.2: ST L3G4200D custom settings.

parameter	Gyroscope range	Acceleration range	Read-out frequency
value	$\pm 75 \text{ deg/s}$	$\pm 2g$	800 Hz

Table 4.3: Murata SCC2000 custom settings. [7]

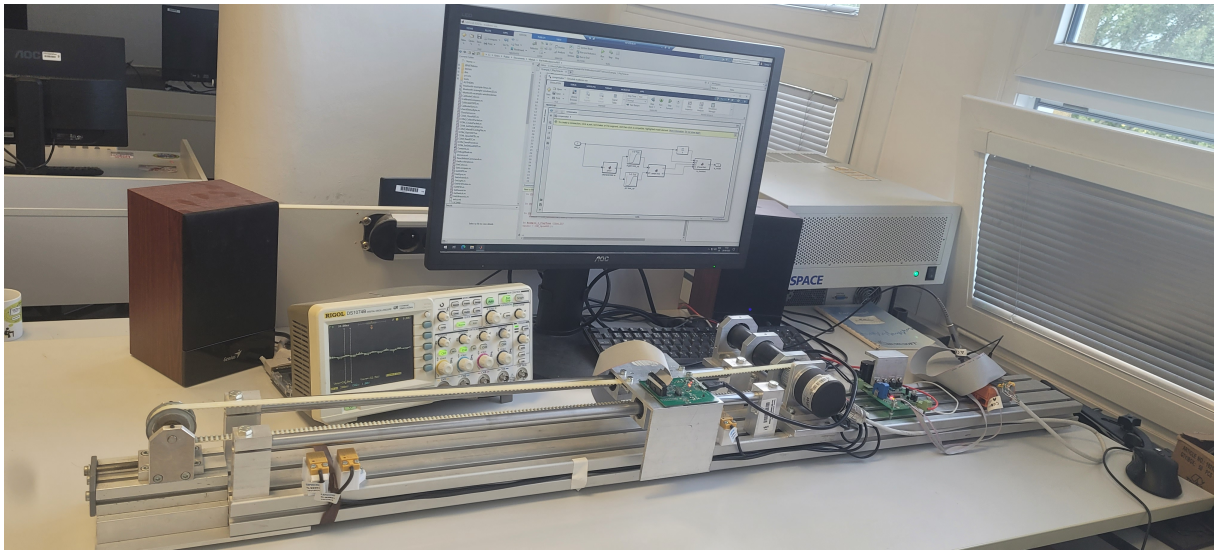


Figure 4.4: Linear movement test-bench.

4.2 Observation A: cross-correlation between same gyroscopic sensors, random excitation

4.2.1 Hypothesis

- **Objective**

Quantify the extent to which linear acceleration and jerk impact gyroscopic measurements.

- **Significance**

Understanding this feature will help us to determine the applicable area for the potential compensators and define the scope of further research.

- **Methodology**

The hypothesis will be tested through a series of controlled experiments designed to isolate and manipulate linear acceleration and angular velocity parameters.

4.2.2 Experiment

By mounting two discrete InvenSense MPU-6050 gyroscopic sensors on a single linear guide, we ensured unidirectional rigid motion along a single axis. In our examination

4 ANALYSIS OF GYROSCOPE MEASUREMENT ERRORS

of the test sample, we pinpointed linear dynamic acceleration and jerk excitations as the predominant error inducers in the gyroscope’s sensing axis—the axis designated for Coriolis force measurements. In this chapter, we focus on the influence of acceleration solely on the sense axis.

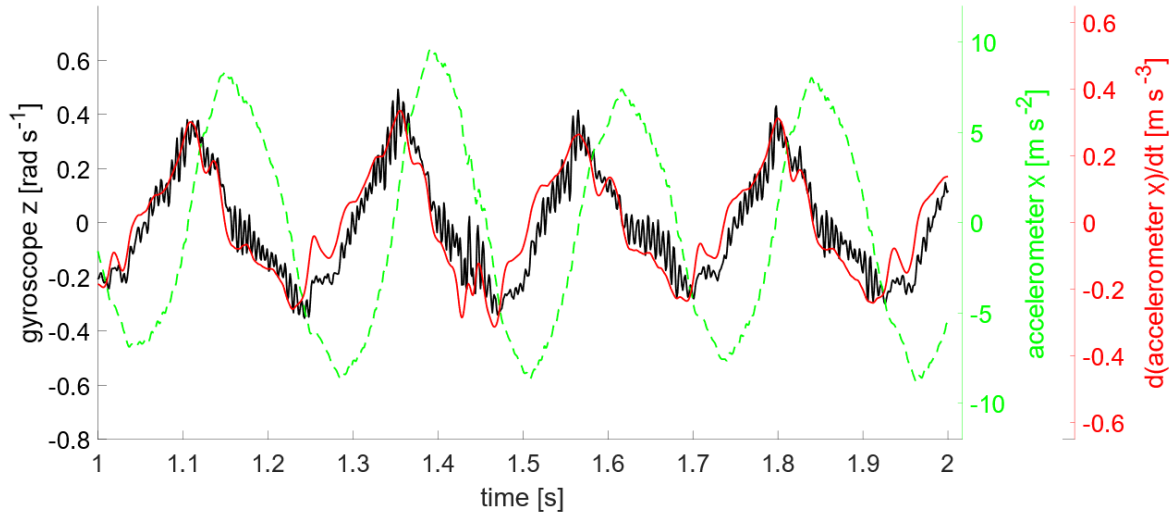


Figure 4.5: Acceleration, jerk, and gyroscope output in the time domain. [3]

The presence of measurement error under conditions of a pseudo constant disturbance frequency is observed to propagate with a phase shift that is directly relative to the correspondingly applied acceleration, as visible in Figure 4.5. Comparing the two inverted sensors demonstrates a deterministic effect of dynamic acceleration disturbances on the gyroscope’s sensing axis. Refer to Figure 4.6 for a time-domain interpretation and Figure 4.7 for signal cross-correlation.

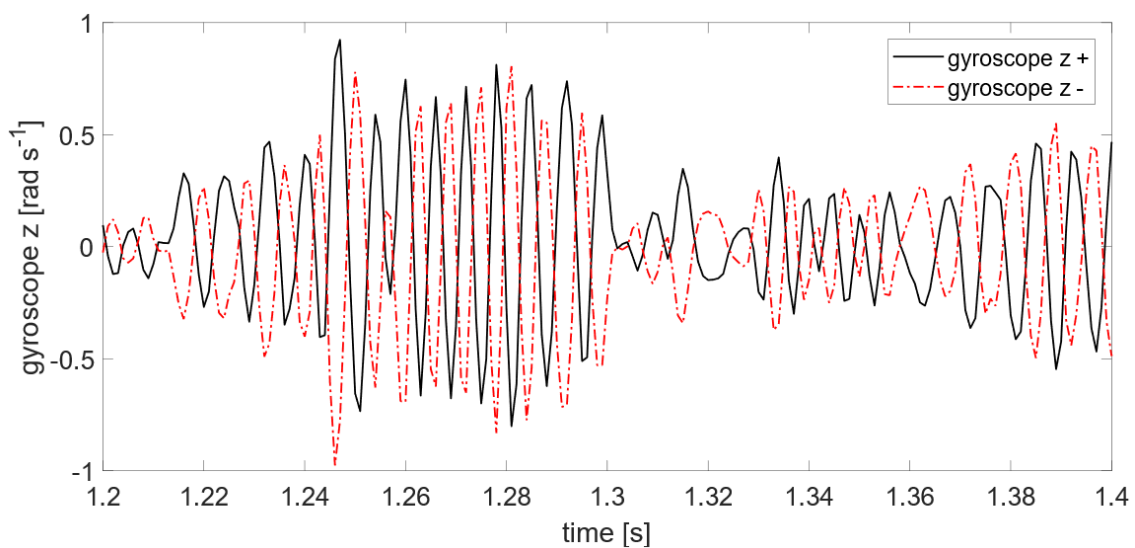


Figure 4.6: Measurement of mechanically coupled gyroscopes. [3]

4 ANALYSIS OF GYROSCOPE MEASUREMENT ERRORS

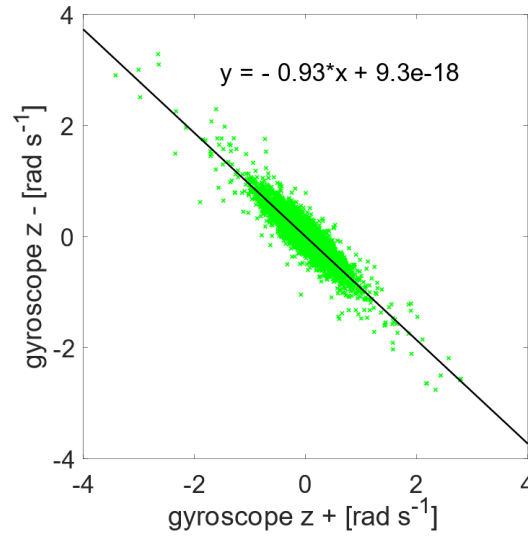


Figure 4.7: Cross-correlation of two identical gyroscopes at zero rotation under dynamic disturbances. [3]

4.2.3 Summary

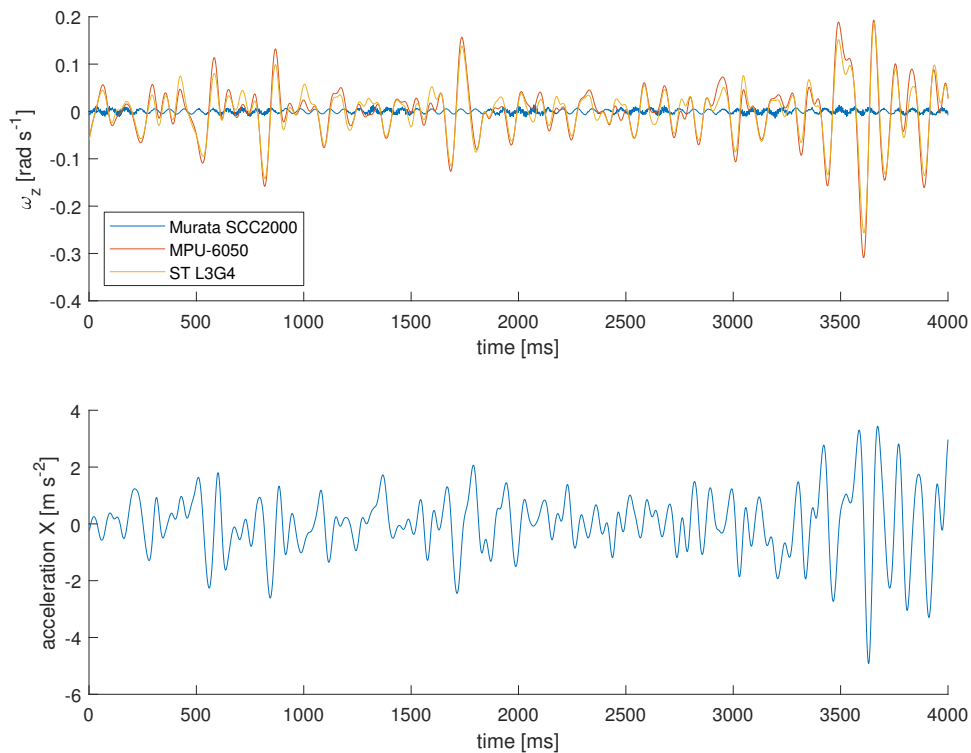


Figure 4.8: Direct comparison of gyroscope sensors affected in sense axis measured under dynamic load.

The observed linear correlation between two gyroscopes that are identical in specification but opposite in orientation lends strong empirical support for the deterministic nature of the phenomenon under investigation. Drawing from the data presented in Figures 4.6

and 4.7, we can robustly validate our initial hypothesis: namely, that mechanical acceleration and corresponding jerk exert a direct, quantifiable impact on the measurements obtained from the gyroscopes sense axis.

4.3 Observation B: cross-correlation between different gyroscopic sensors, random excitation

4.3.1 Hypothesis

- **Objective:** Empirically analyze how linear acceleration in each orthogonal direction affects the measured output of various MEMS gyroscopic sensors.
- **Significance:** Understanding this feature could lead to improvements in MEMS gyroscopic sensor accuracy which could lead to more robust error-correction algorithms for these sensors.
- **Methodology:** Collect data using multiple MEMS gyroscopic sensors under varying conditions of linear acceleration and jerk.

4.3.2 Experiment

Specifically, the gyroscopic sensors examined in this section encompass:

- InvenSense MPU-6050
- ST L3G4200D
- Murata SCC2000

During the experimental phase, a nuanced observation was made. Accelerations in orthogonal axes, that are the drive axis and the sense axis, exert divergent influences on the gyroscopic measurements. Consequently, our initial task was to address the spatial orientations of these sensor axes of selected gyroscopes. The primary metric for evaluation in this context was variance in axis-specific sensitivities.

This experimental protocol builds upon previous research findings [3], which have demonstrated that dynamic excitation along the sensing axis contributes to gyroscopic measurements at a magnitude approximately five times greater than that along the drive axis.

For the two selected sensors, we notice that the propagation of dynamic disturbances in the sensing direction of the gyroscope to its output is almost identical, based on the evaluation of linear fit R^2 between both gyroscopes. Comparing the Zero Rate Outputs (ZRO) of both gyroscopes in a single graph, we can get meaningful insights into the similarities in the performance of both sensors under identical conditions, see Figure 4.9. The closer the value of R^2 is to 1, the more deterministic the response of the gyroscopes to identical input. It is evident that, in the first case as referenced in Figure 4.11, the linear fit R^2 is 0.95, revealing the same behavior of both sensors.

When dynamic disturbance was introduced in the orthogonal direction, specifically the drive axis, in Figure 4.10, the response of both sensors did not align as well, showing

4 ANALYSIS OF GYROSCOPE MEASUREMENT ERRORS

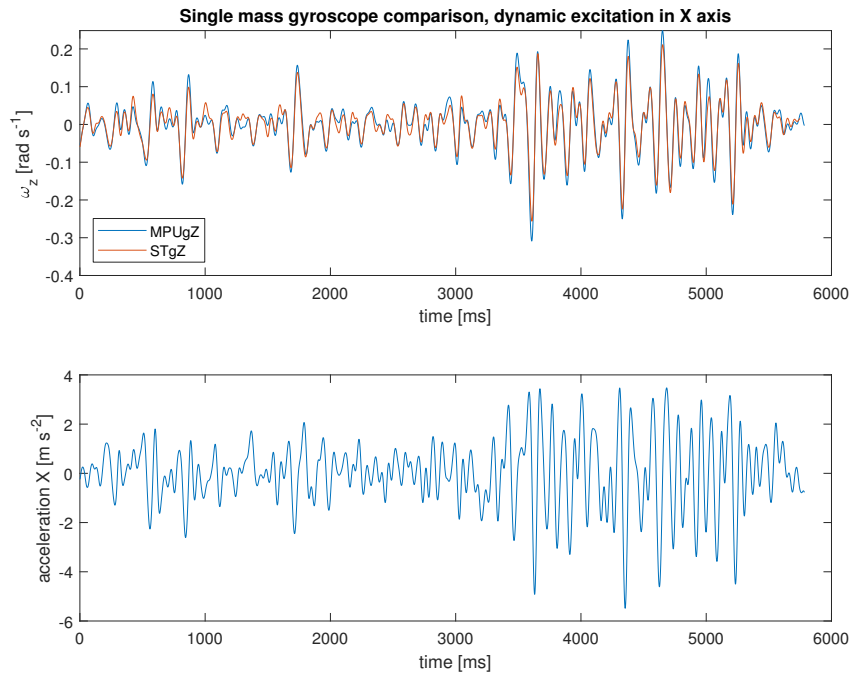


Figure 4.9: Single mass gyroscopes comparison, X axis dynamics.

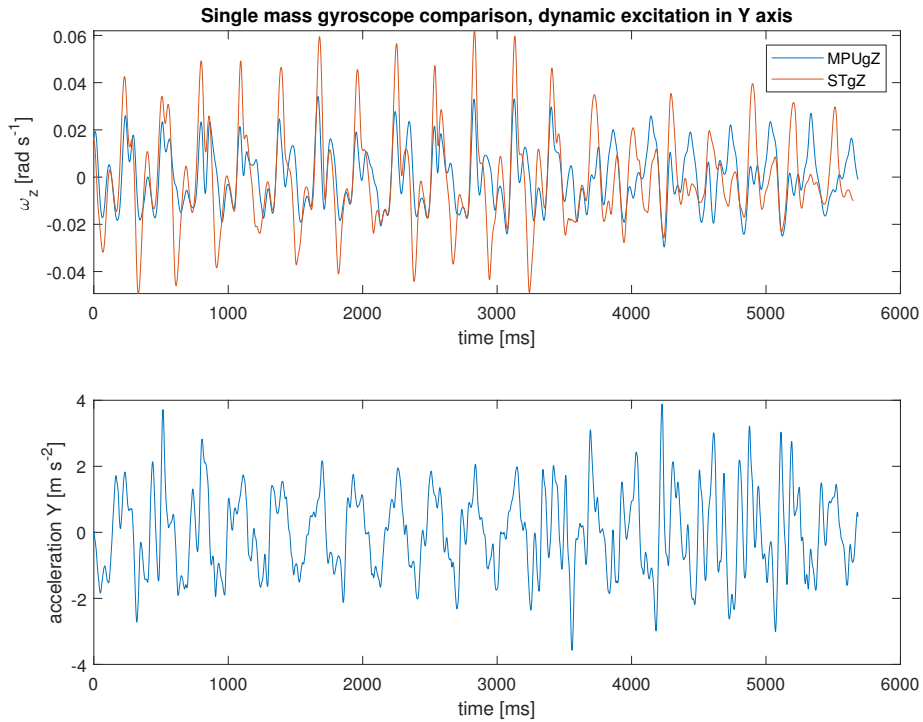


Figure 4.10: Single mass gyroscopes comparison, Y axis dynamics.

a R^2 value of 0.34, as in Figure 4.12. This behavior might be attributed to the active mode-matching technique employed in the MEMS gyroscope design, implying that the gyroscope is modulating the resonant frequency to offset the induced disturbance. However, such design specifics are not disclosed in the datasheet. Consequently, the deterministic

4 ANALYSIS OF GYROSCOPE MEASUREMENT ERRORS

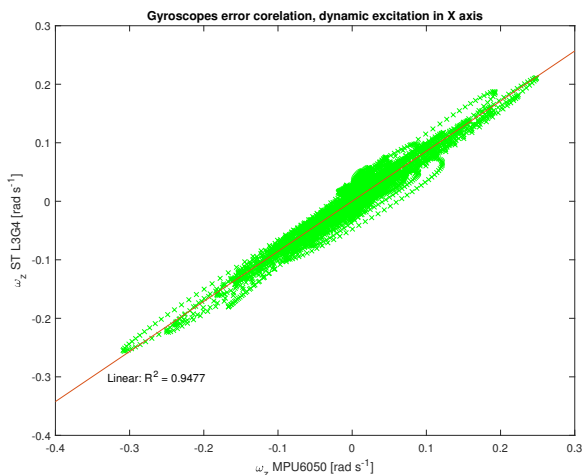


Figure 4.11: Correlation of two single mass gyroscopes, X axis dynamics.

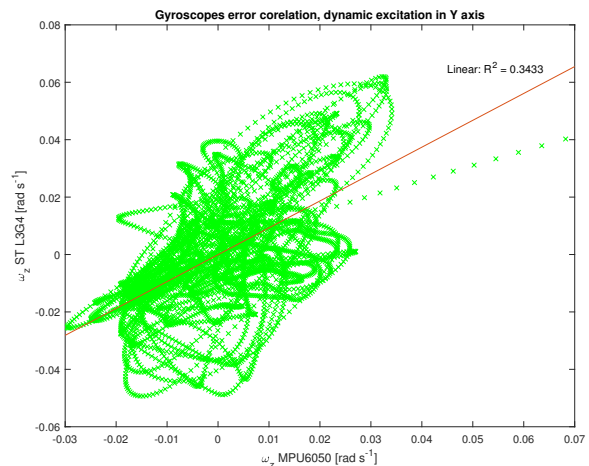


Figure 4.12: Correlation of two single mass gyroscopes, Y axis dynamics.

behavior is not as strong as it is in the sense axis.

Comparison with dual-mass MEMS gyroscope

Upon analyzing time-domain graphical data, in the following Figures 4.13, it was evident that the Murata dual mass gyroscope’s output remained largely unaltered in response to external force applications. Owing to the fact that we opted for data acquisition at the maximum allowable frequency, no filtering mechanisms were implemented, consequently, periodic noise is visible in the output graphs. Even when subject to external dynamic perturbations, the gyroscope’s measurement demonstrated remarkable stability, deviating minimally from baseline levels, direct comparison in Figure 4.8.

Thus, we posit that these gyroscopes are inherently less vulnerable to disruptions caused by linear acceleration on the sensing axis, a claim that is supported by comparative data visualized in subsequent Figures 4.13.

4.3.3 Summary

Visualized measurements were repeatedly conducted with the results written in Table 4.4. Considering the comprehensive dataset acquired through our experiments, we can assertively conclude that the dynamical effects exert a pronounced influence on gyroscope measurements, particularly along the sensing axis. Specifically, when subject to dynamic excitations in the ‘X’ axis—which we have identified as the sensing axis—the error propagation into the measurement output is markedly present. Moreover, our data elucidates that the error propagation along the sensing axis is approximately five times more potent than when the same dynamic influences are applied along the drive axis.

R^2 of ω_z	1	2	3	4	5	6
X axis disturbance	0.9477	0.9612	0.9388	0.9547	0.9496	0.9569
Y axis disturbance	0.3433	0.2863	0.4201	0.3755	0.3311	0.4187

Table 4.4: R^2 values for different sets of data.

The antiparallel movement of dual mass MEMS gyroscope and differential signal processing effectively acts as a compensatory mechanism, mitigating distortions that would

4 ANALYSIS OF GYROSCOPE MEASUREMENT ERRORS

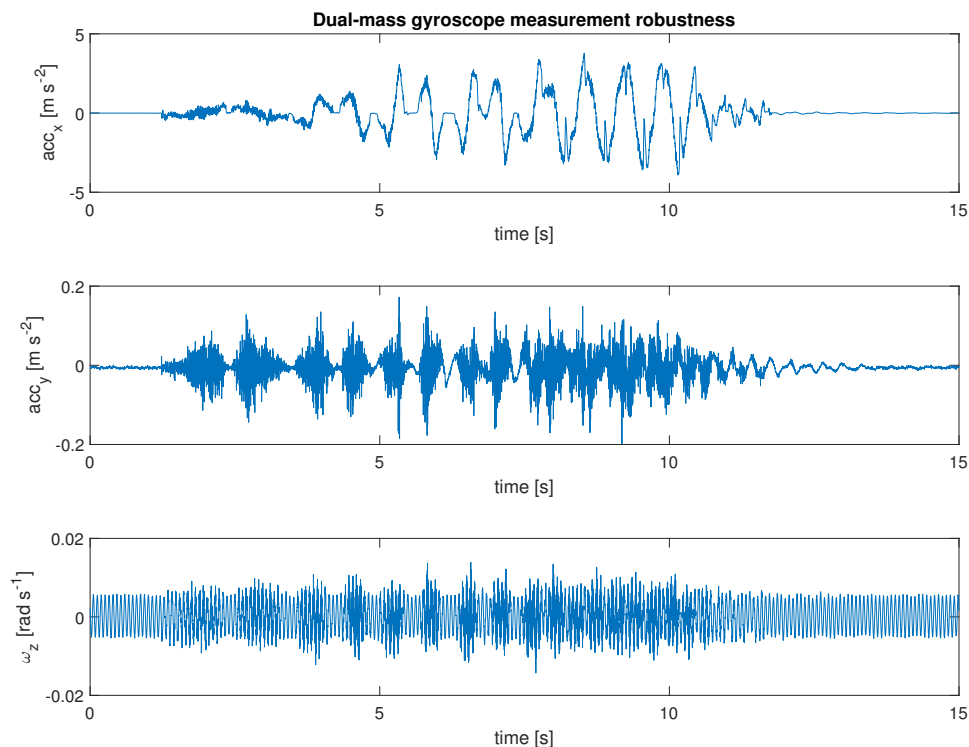


Figure 4.13: Murata SCC2000 IMU performance. X axis disturbance

otherwise introduce significant biases as in single-mass systems. As a result, the dual-mass MEMS gyroscope exhibits a remarkable capacity for maintaining rigid and stable measurements, thereby substantively diminishing the susceptibility to external parasitic influences that frequently plague its single-mass counterparts.

4.4 Observation C: different gyroscopic sensors, wide range of excitations

To assess the sensitivity of the gyroscopic sensor to linear accelerations across a frequency spectrum ranging from single to ten of Hz, we employed a dedicated measurement approach, potentially extendable to user-defined frequency resolution. Acceleration metrics were directly gauged using a triaxial accelerometer, which was synchronized with the gyroscopic output data.

Our empirical data unambiguously reveal a highly consistent pattern of error across single-mass gyroscopic sensors. Specifically, when these sensors are subjected to harmonic translational motions with a sinusoidal profile, they provide a non-zero angular velocity. This behavior not only shares the frequency of the original sinusoidal excitation but also manifests with a distinct amplitude and a predictable phase shift relative to the excitation itself.

Upon evaluation of the single-mass MEMS gyroscope, it becomes evident that both acceleration and jerk have a direct and deterministic influence on the sensor's measurements. This was examined by applying targeted linear accelerations along the sensing axis of the gyroscopic sensor. In these controlled experiments, we observed a systematic

4 ANALYSIS OF GYROSCOPE MEASUREMENT ERRORS

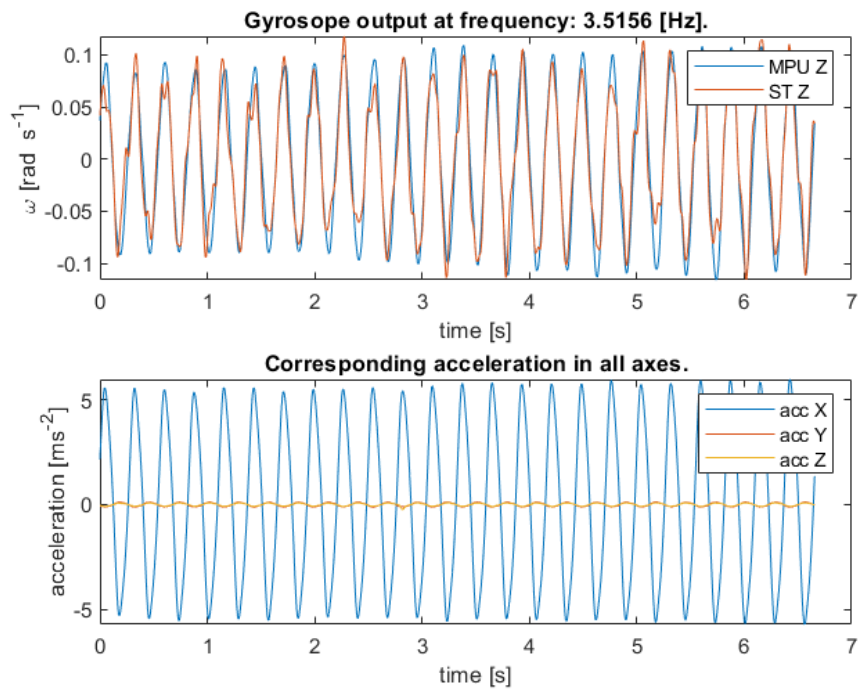


Figure 4.14: Sinusoidal harmonic excitation 3.5 Hz.

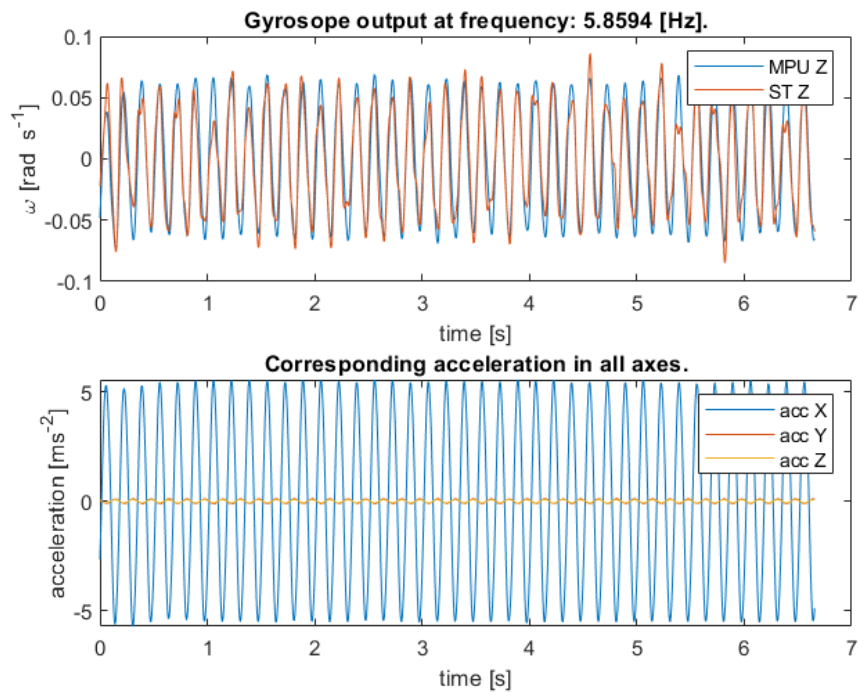


Figure 4.15: Sinusoidal harmonic excitation 5.9 Hz.

bias in the sensor's output, affirming that the distortions were not stochastic but followed a well-defined pattern.

5 Compensational models

In our experimental evaluation, we examined two distinct types of compensation algorithms:

- A nonlinear model parameterized via the nonlinear least squares method, which allows for precise tailoring of the model to fit observed system behavior.
- An artificial neural network-based model, which leverages machine learning techniques to adaptively correct for undesired gyroscope responses.

5.1 Non-Linear Least Squares

Utilizing the nonlinear least squares methodology, we estimated the model parameters by invoking a specific harmonic equation of motion as our foundational analytical framework in Chapter 4. This approach allows for an optimal parameterization that maximizes the fidelity between the empirical observations and the theoretical constructs. The harmonic equation serves as a critical mathematical representation that encapsulates the system's dynamic behavior, providing a robust basis for subsequent analyses and predictions. Having a harmonic acceleration disturbance y_{acc} :

$$y_{acc}(t) = A_a \sin(2\pi ft) \quad (5.1)$$

We observe the gyroscope signal $y_{gyroZRO}$:

$$y_{gyroZRO}(t) = A_g \sin(2\pi ft + \varphi_g) \quad (5.2)$$

, where A_a stands for the acceleration amplitude of excitation, A_g stands for the amplitude of the ZRO gyroscope, f for the frequency of the harmonic signal and φ_g the ZRO phase change. In such a situation we can consider the jerk also smooth and harmonic.

Our observations leads us to the necessity of finding the transfer function between dynamical disturbance measured by the accelerometer and the gyroscope's zero rate output, such that:

$$y_{gyroZRO}(s) = F(s)y_{acc}(s) \quad (5.3)$$

, where $F(s)$ can be considered as a feedforward compensator model in the s-domain. In the scope of our work, we could think about the gyroscope measurement such that:

$$\omega_{gyro} = \omega_{real} + y_{gyroZRO} + y_{errors} \quad (5.4)$$

5 COMPENSATIONAL MODELS

, where ω_{gyro} is MEMS gyroscope measurement, ω_{real} is real angular rotation, $y_{gyroZRO}$ is the error caused by dynamic disturbance, and y_{errors} are other error terms out of the scope of this work.

In the discrete form we propose to derive the $y_{gyroZRO}$ as in equation 5.5.

$$y_{gyroZRO}[n] = A(f)y_{acc}[n - \varphi(f)] \quad (5.5)$$

, where n is the sample number in a discrete system, $A(f)$ is the compensation parameter of the amplitude as a function of the frequency of the harmonic disturbance, and $\varphi(f)$ is the phase shift as a function of the frequency of the harmonic disturbance.

As the phase shift is a parameter of a non-linear function, sinus, the NLS algorithm has to be involved in the evaluation of the error model. Besides the phase shift, the error was accompanied by fluctuating amplification levels contingent upon the frequency of the oscillations, such a dependency is clearly linear.

As a testament to the efficiency and precision of this optimization-based methodology, some of the findings, notably capturing trends in amplitude, frequency, and phase shift, have been described through graphical visualizations presented in the Figures 5.1 and 5.2. Such dataset and accompanying analysis serve as a comprehensive empirical foundation.

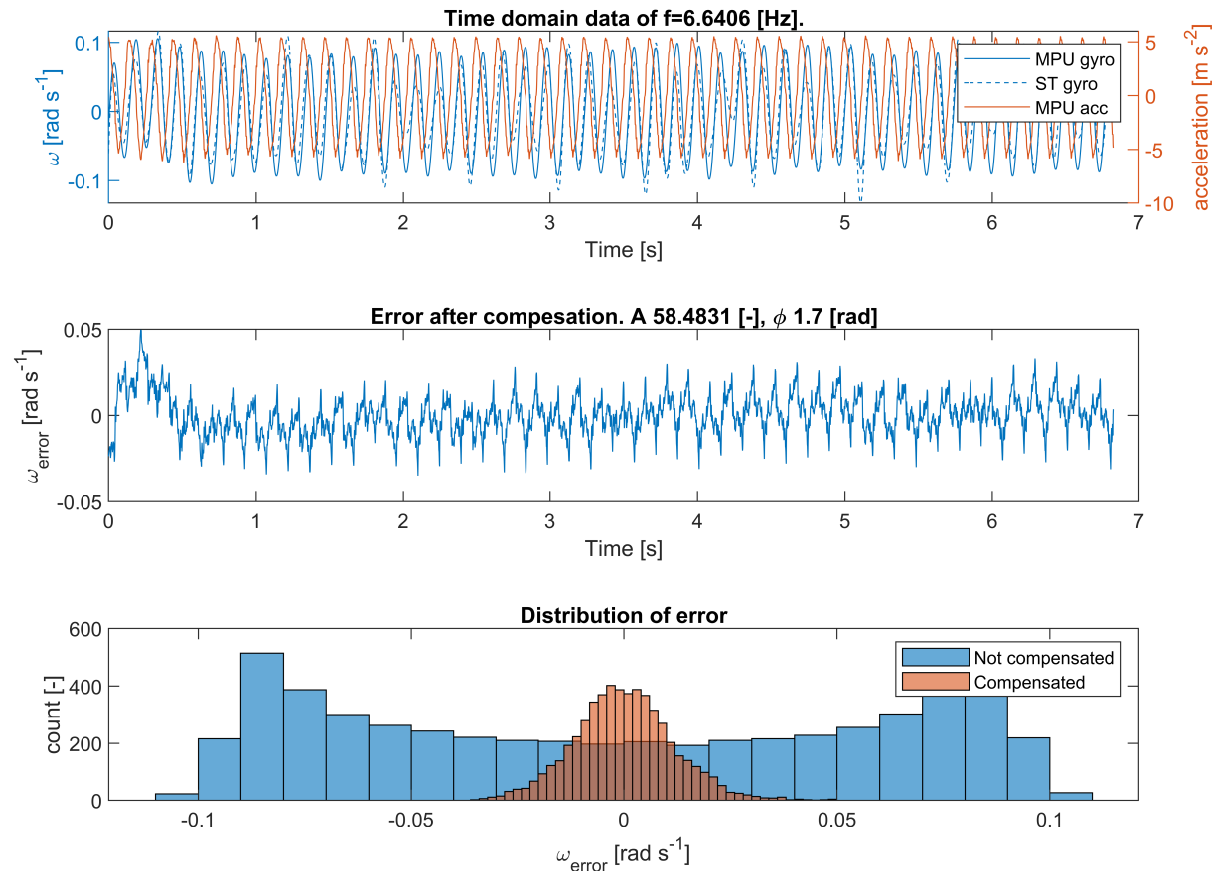


Figure 5.1: Sine harmonic excitation 6 Hz.

The post-compensation error distribution ought to exhibit Gaussian characteristics for the model to be deemed valid, in Figure 5.3. Gaussian-like behavior in the error distribution becomes markedly consistent for frequencies exceeding 3.5 Hz.

5 COMPENSATIONAL MODELS

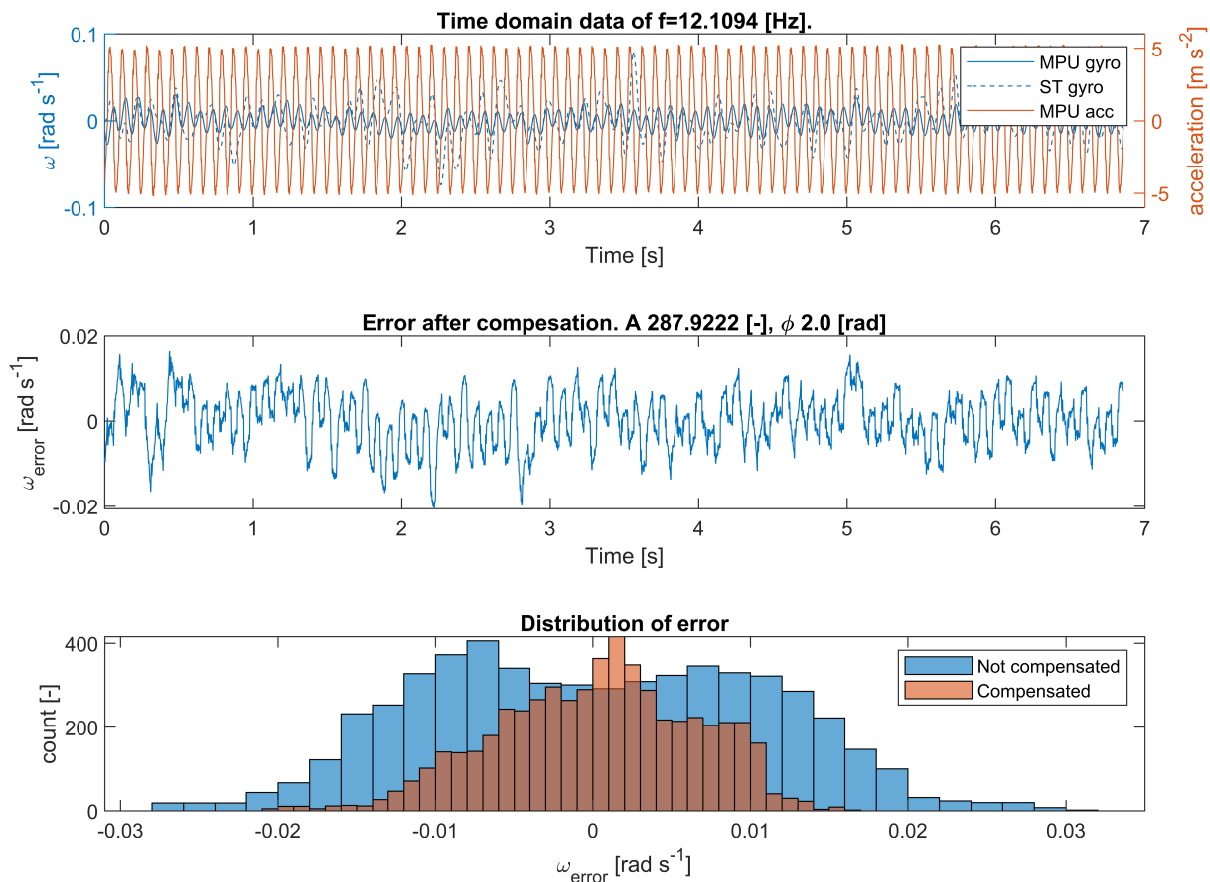


Figure 5.2: Sine harmonic excitation 12 Hz.

Conducting a comparative analysis, it becomes evident that the compensatory mechanism exerts a significant suppression of error, respectively the standard deviation of the Zero Rate Output (ZRO) under dynamic disturbances beyond the frequency of 3.5 Hz, see Figure 5.5. This suggests that the compensator is particularly effective in mitigating dynamic disturbances in frequencies between 3 to 12 Hz and potentially beyond, thereby stabilizing the ZRO's variability. This observation is pivotal, not only for substantiating the compensator's utility but also for delineating the frequency-dependent operational boundaries where the system exhibits optimal performance.

Based on our data assessment, we would propose the storage of compensator parameters in a look-up table (LUT) equipped with linear interpolation functionalities for in-between data points. This structure offers an optimized solution for potential embedded systems by enabling rapid parameter retrieval and computational efficiency—a crucial requirement given the resource limitations typical in embedded environments. For future investigations, we have identified an intriguing pattern in the behavior of the gain parameter, which serves as the direct conduit for the propagation of acceleration signals to the gyroscope output. Specifically, the gain parameter manifests a quadratic growth trajectory, with the quadratic minima located around a frequency of 3.5 Hz. Below frequency of 3.5 Hz, i.e. quadratic minima, we have applied constant parameter A. In the context of phase shift parameters, our preliminary analysis reveals a linearly ascending trend across the measured dataset. The evolution of both parameters on frequency is in Figure 5.6.

5 COMPENSATIONAL MODELS

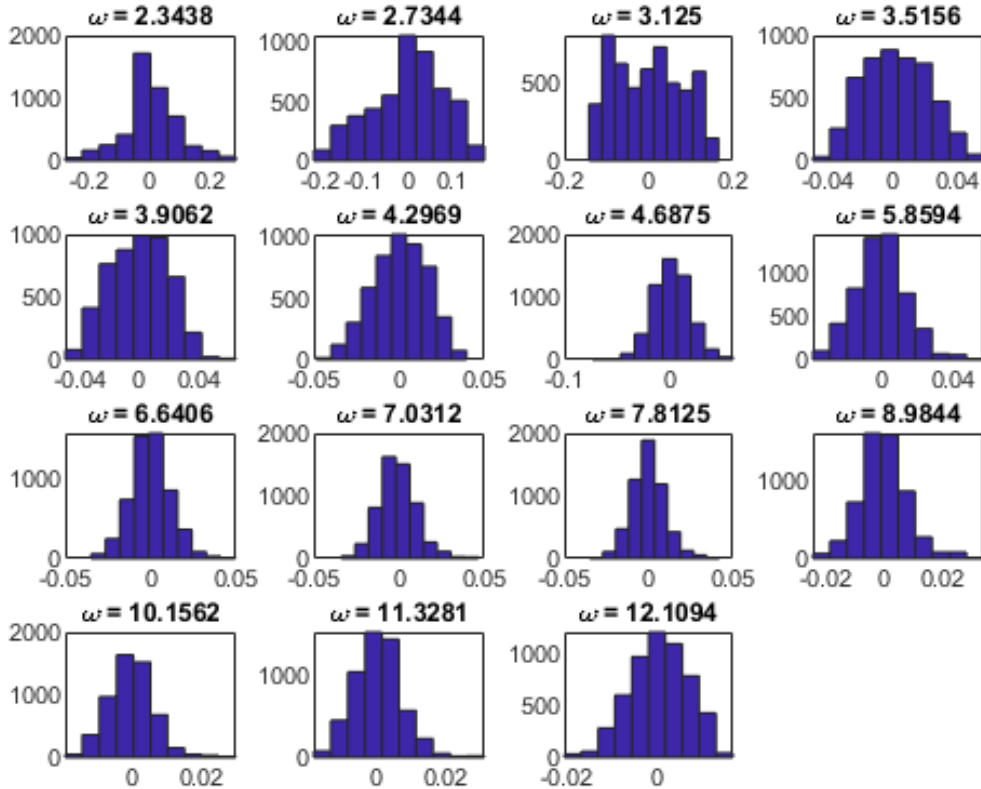


Figure 5.3: Histograms of error across multiple frequencies.

$\omega[Hz]$	3,13	3,52	3,91	4,30	4,69	5,86	6,64	7,03	7,81	8,98	10,16	11,33	12,11
Skewness	0,13	0,11	-0,02	-0,18	-0,03	0,24	0,24	0,48	0,28	0,38	0,44	0,42	-0,25
Kurtosis	1,83	2,27	2,36	2,48	3,44	3,36	3,53	3,92	3,71	3,82	4,16	3,83	2,70

Figure 5.4: Characteristics of compensated error.

5.2 Artificial Neural Network - ANN

As a complementary method for addressing zero-rate output gyroscope error compensation, more sophisticated methodologies, such as artificial neural networks, were explored. In our prior research [3], we have achieved a promising compensatory framework by employing a nonlinear autoregressive neural network with feedback loops.

As of the present moment, there exists no universally accepted methodology for definitively determining the optimal complexity of an artificial neural network.

In the context of our specific problem, we are working with a single-input, single-output topology where the input represents acceleration along a specific axis, and the output models the error associated with a gyroscope. The primary question revolves around the architecture of the hidden layers and the potential necessity for feedback mechanisms within the network.

One critical constraint to consider is the real-time hardware implementation, particularly with a focus on Field-Programmable Gate Arrays. Specifically, we intend to utilize the Xilinx ZYNQ 7000 series. This FPGA family offers a resource range consisting of

5 COMPENSATIONAL MODELS

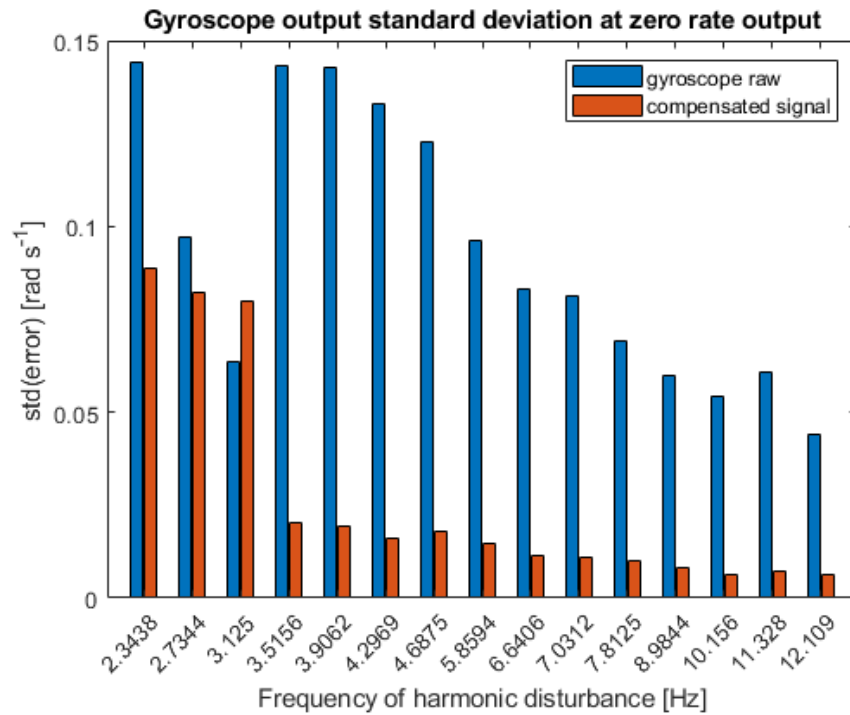


Figure 5.5: Comparison of ZRO output. With and without compensator.

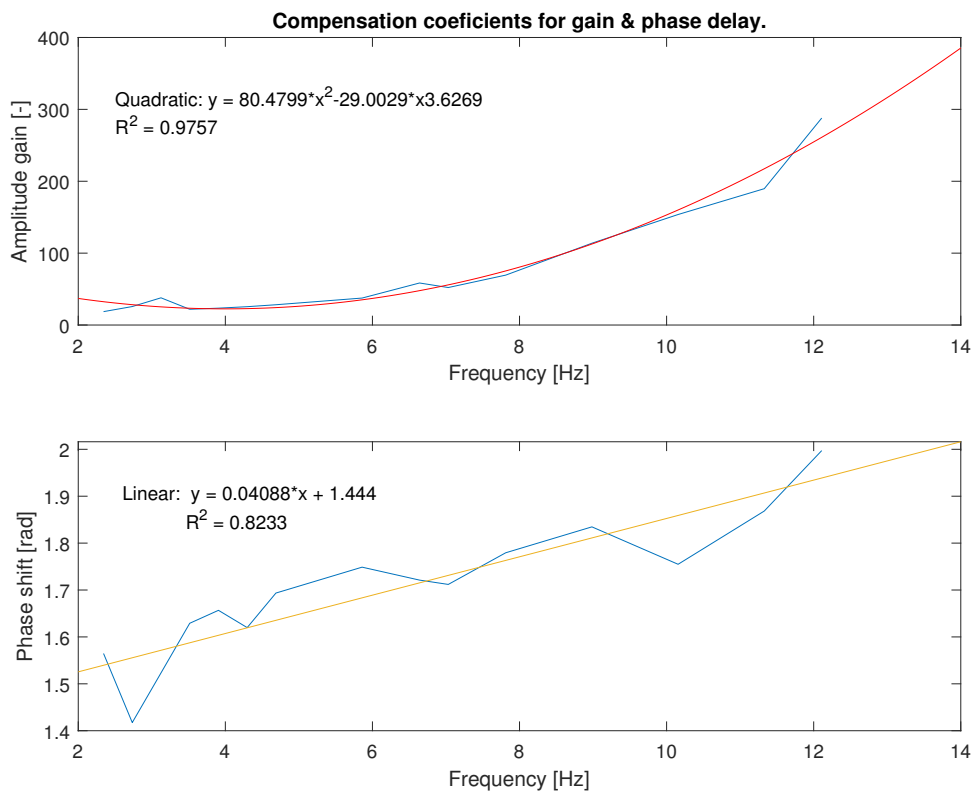


Figure 5.6: Evolution of compensator parameters for 5 ms^{-2} acceleration amplitude.

several hundred to upwards of 2000 Digital Signal Processing (DSP) slices. This information is instrumental in defining not only the dimensions of the hidden layers but also the

5 COMPENSATIONAL MODELS

degree of interconnectivity within the network.

- **Multiplication:** DSP slices that are optimized for multiplication operations. A single multiplication can be done in one DSP slice.
- **Addition:** Adders are usually simpler and can be implemented in the FPGA's general logic slices. A single adder might consume a few LUTs (Look-Up Tables) and Flip-Flops (FF) within a slice.
- **Wires and Routing:** Interconnections also consume routing resources, although these are generally harder to quantify than logic or DSP slices.

Considering these points, one interconnection might consume the following:

- 1 DSP slice for multiplication.
- A few LUTs and FFs for the addition.

Layer A consisting of N_a neurons interfacing the layer B consisting of N_b neurons combinatorically result into n_{ab} interconnection such that:

$$n_{ab} = N_a N_b \quad (5.6)$$

Having more than two layers:

$$n_{a\dots i} = \sum_{i=m}^n N_m N_{m+1} \quad (5.7)$$

As we have available 2000 DSP slices, we selected the 4-layer structure with 30, 30, 20, and 10 neurons in each layer as the most complex, resulting in 1700 interconnections inside the hidden layer and so the adequate amount of DSPs.

5.2.1 NN definition and training

To systematically explore the architecture space for an optimal neural network configuration tailored to our specific task, we devised an automated grid search algorithm. This algorithm programmatically iterates through a predefined set of neural network structures, as outlined below:

1. Initiate the search with a single-hidden-layer neural network containing 10 neurons.
2. Incrementally increase the neuron count in that layer by 10, up to a maximum of 30 neurons.
3. Introduce feedback connections from the last layer back to the first layer and evaluate the performance of these recurrent architectures.
4. Add an additional hidden layer and execute a combinatorial search across various neuron counts in each layer, both with and without feedback connections.
5. Continue this iterative process until the architecture reaches a complexity of four hidden layers, each containing up to 30 neurons, complete with feedback loops where specified.

5 COMPENSATIONAL MODELS

Our empirical evaluations substantiate this preference: the four-hidden-layer ANN without feedback, in Figure 5.7 not only mitigated the issue of time delays but also outperformed its feedback-enabled counterpart in key performance metrics.

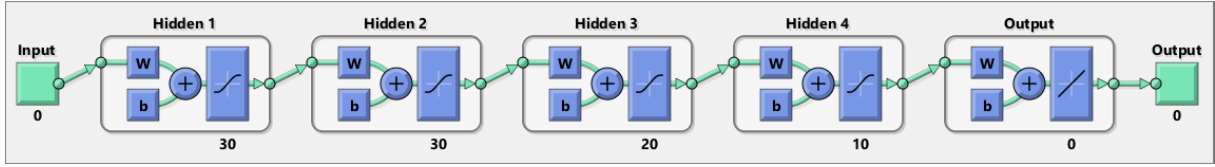


Figure 5.7: Illustrative neural network model without feedback.

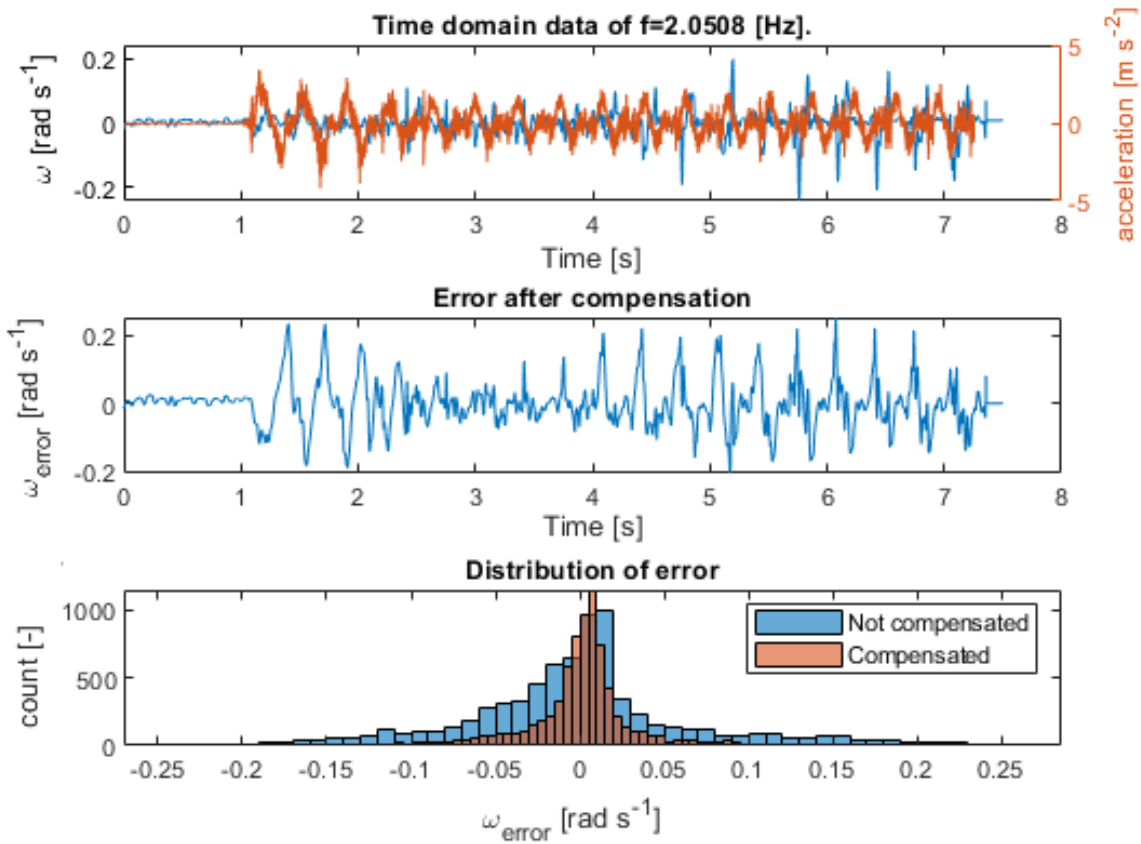


Figure 5.8: Exemplary data of 4-layer, 120 neuron mesh.

The artificial neural network did exhibit some efficacy in mitigating errors, particularly within lower frequency bands. A representative example of this performance enhancement can be observed in Figure 5.8. In this illustration, the key performance indicator under scrutiny is the standard deviation of the error, which is readily discernible from the associated histogram located at the bottom of the Figure.

The histogram of standard deviations serves as an empirical validation of the model’s capability to suppress zero rate output, thereby underscoring the network’s partial success in refining the gyroscope’s Zero Rate Output within specific frequency ranges. While this doesn’t negate the challenges we’ve outlined with respect to broader frequency ranges, it does suggest that the ANN approach holds promise and merits further investigation for targeted frequency suppression.

However, as illustrated in Figure 5.9, even the most intricate artificial neural net-

5 COMPENSATIONAL MODELS

work architecture within our search purview failed to comprehensively compensate for the zero rate output of the gyroscope across the entire spectrum of dynamic disturbances. Intriguingly, at certain frequencies, the standard deviation of the compensated signal deteriorated, performing worse than the original, uncompensated signal.

These observations underscore the need for a more nuanced approach to ANN design and training, specifically tailored to tackle the challenges presented by the dynamic disturbances affecting gyroscope measurements.

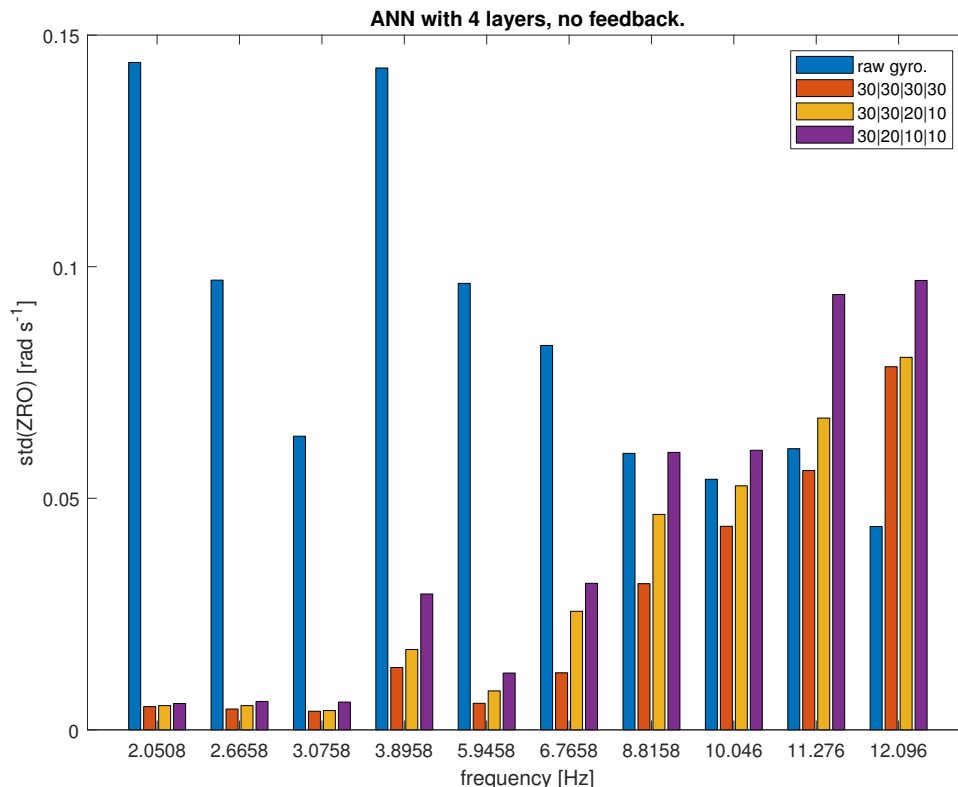


Figure 5.9: Comparative performance of 4 layers meshes, without feedback.

5.3 Summary

For the purpose of this study, we focused on periodic signals with acceleration amplitudes up to 5 ms^{-2} and within a frequency range spanning from 2 Hz to 12 Hz . We employed standard deviation as our principal metric to assess the efficacy of the compensatory algorithms, as in an ideal state of no rotation, the standard deviation of the compensated gyroscope under dynamic disturbance should stay 0 rads^{-1} .

While neither compensatory algorithm could comprehensively address disturbances across the entire frequency spectrum, they did exhibit complementary strengths on opposite sides of the frequency region of interest. Potential synergic interplay suggests the utility of integrating both methods into a single, robust compensatory framework. However, it's worth noting that the ANN-based approach poses significant computational challenges, especially when considering its implementation on conventional FPGA platforms, where resource constraints might limit the complexity of the neural network that can be deployed.

6 Implementation on RT HW

In our research setup, we employed an automated code generation process through a cohesive toolchain that integrates several software and hardware components. On the software end, the toolchain encompasses the MathWorks suite, including Matlab, Simulink, Matlab Coder, Simulink Coder, and Embedded Coder. Additionally, we utilized MPLAB Device Blocks for Simulink, to facilitate code generation compatible with Microchip hardware. From the Microchip set of tools we used the compiler MPLAB XC, MPLAB X IDE, microcontroller programmer PicKit and microcontroller itself. The microcontroller applied is a dsPIC33FJ128MC804.

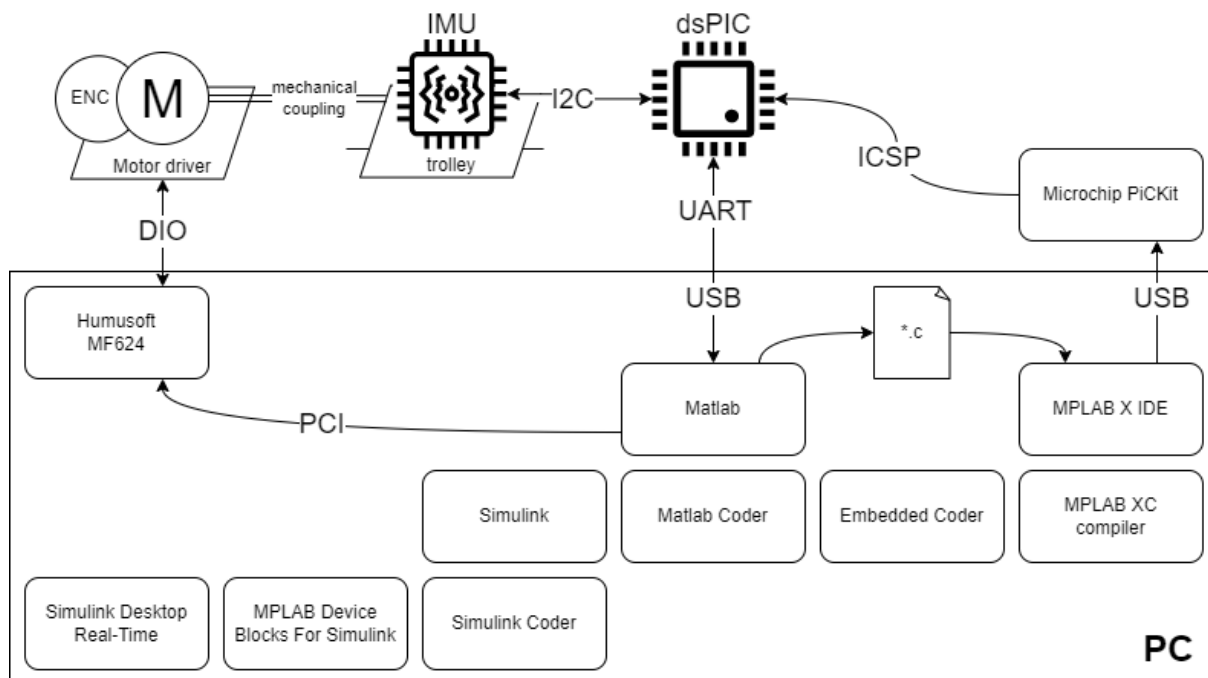


Figure 6.1: Schematic of the system used for prototyping and research.

6.1 Artificial neural network algorithm

In the proposed design, we consider implementing an artificial neural network comprising four layers with respective neuron counts of 30, 30, 20, and 10. The weight matrices \bar{W} are dimensioned as 30×30 , 30×20 , and 20×10 , necessitating the storage of 1700 weight parameters. The target operational frequency for this network is 800 Hz .

A computationally demanding aspect of this network is the matrix-vector multiplication. To elaborate, a single dot product operation for one row in a 30×30 matrix requires 30 multiplications and 29 additions, summing up to 59 computational operations. When this is scaled for the entire matrix, we arrive at 1770 operations. On the dsPIC33FJ128MC804 microcontroller, each of these operations involves 2 instructions

for loading the numbers, 1 for multiplication, and 1 for storing the result—a total of 4 instructions per operation.

Extrapolating these requirements to an 800 *Hz* operational frequency, the computational load for just the first layer alone reaches approximately 5.6 Million Instructions Per Second (MIPS), which already exceeds the microcontroller’s processing capabilities, which is 3.6 MIPS in standard.

6.2 NLS-based compensator implementation and performance

For the successful real-time deployment of our proposed algorithm on hardware, it is imperative to carefully consider the computational constraints intrinsic to embedded systems. These constraints predominantly encompass memory capacity and the computational latency associated with the execution of complex, non-linear functions. To circumvent these limitations, we advocate for the adoption of a compensation algorithm founded on a look-up table (LUT) infrastructure. This LUT will house precomputed values that have been empirically determined through system identification techniques, as delineated in the section 5.1. The integration of phase shift calculations into our compensatory algorithm presents a particularly intricate challenge, especially when computational efficiency is paramount. A general sinusoidal function—in our case phase shifted response of gyroscope:

$$A \sin(2\pi ft + \varphi) = y_{gyroZRO}(t) \quad (6.1)$$

can be rewritten using trigonometric identities into the form, which is a sum of weighted sine and cosine terms:

$$A(\sin(2\pi ft) \cos(\varphi) + \cos(2\pi ft) \sin(\varphi)) \quad (6.2)$$

where, $A \cos(\varphi)$ and $A \sin(\varphi)$ are the weights for the $\sin(2\pi ft)$ being measure and $\cos(2\pi ft)$ numerically derived. By adjusting the weights $A \cos(\varphi)$ and $A \sin(\varphi)$, you can effectively implement a phase shift φ in the original sinusoidal function. This form is particularly useful in signal processing and control systems, as it enables easier analysis and manipulation of sinusoidal signals.

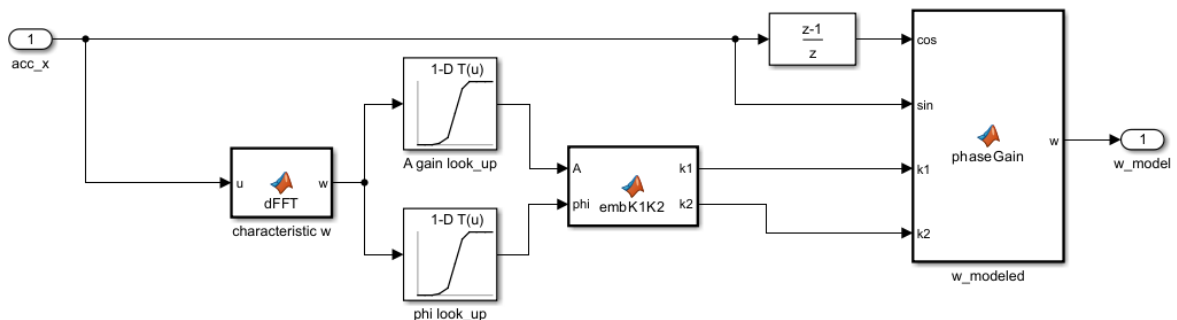


Figure 6.2: Basis of embedded Simulink model.

According to our previous work [4] we have extended the proposed algorithm to facilitate our latest findings, summarized in Figure 5.6 regarding the dependency of amplitude gain and phase shift to the dynamic disturbances to the model as described on the illustration 6.2.

6 IMPLEMENTATION ON RT HW

To obtain the desired compensator functionality following pseudocode can be applied:

1. Determine the gain and phase shift from look-up table, to apply.
2. Multiply original $\sin(2\pi ft)$ from accelerometer by A and $\cos(\varphi)$.
3. Numerically derive the original acceleration signal, preferably applying Savitzky-Golay filter.
4. Multiply the result of point 3. by A and $\sin(\varphi)$.
5. Sum the results of steps 2 and 4, to get phase shifted signal as stated in Equation 6.2.

This way allows us to define a phase shift and amplitude by the sum of two complementary functions.

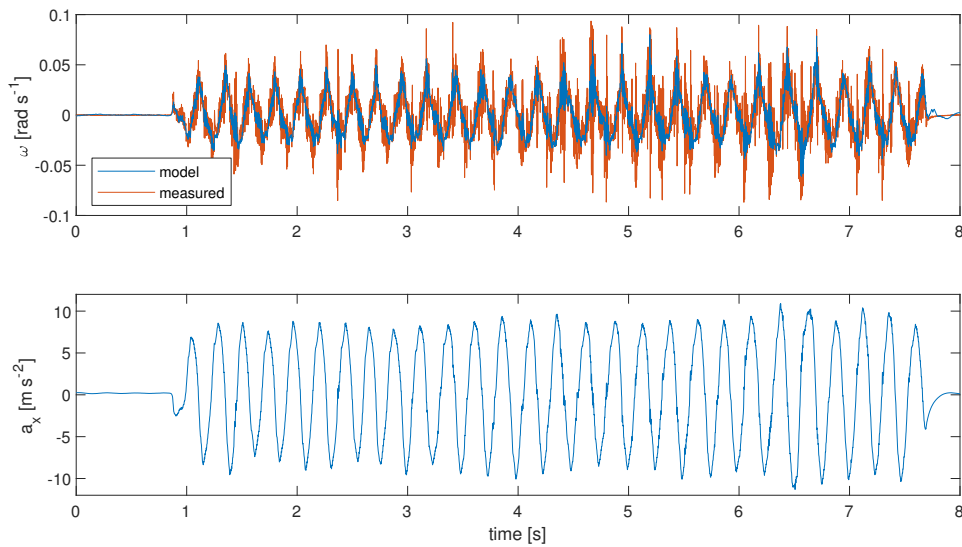


Figure 6.3: Measured and modelled gyroscope error.

Modeled ω could be used to compensate for the actual raw measurement of the gyroscope as defined:

$$\omega_{\text{compensated}}(t) = \omega_{\text{gyro}}(t) - y_{\text{gyroZRO}}(t) \quad (6.3)$$

The compensated measurement was read out from microcontroller after processing with the following result. Illustrative performance can be seen in Figure 6.3 with compensator performance visible in Figure 6.4. Read-out values were processed by the microcontroller onboard in real-time.

Post-processing the data has identified the following performance of the algorithm summarized in Table 6.1.

	ω_{gyro}	$\omega_{\text{compensated}}$
mean [rad/s]	$1.4056e - 16$	$1.566e - 14$
standard deviation [rad/s]	0.1328	0.0151

Table 6.1: Compensator error comparison.

Of greater consequence is the performance of our algorithm in relation to the standard deviation of error, particularly under harmonic disturbances. Our observations demonstrate that the algorithm has achieved a substantial reduction in standard deviation—on

6 IMPLEMENTATION ON RT HW

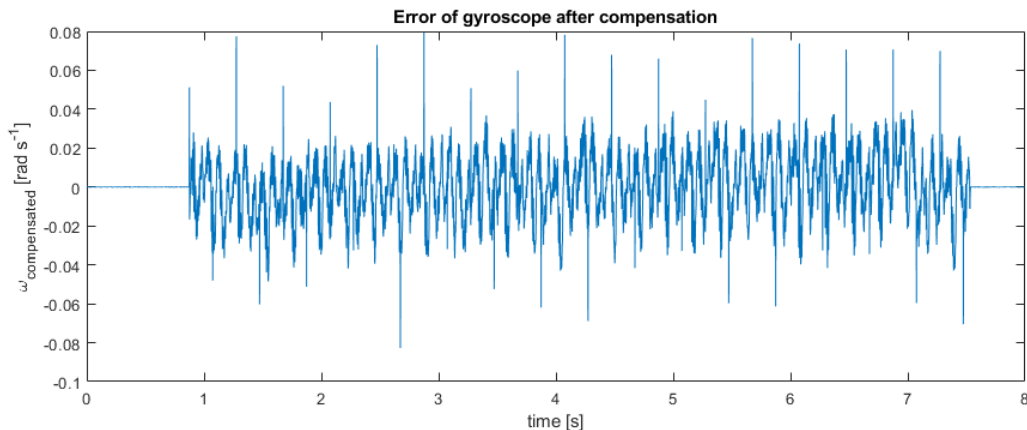


Figure 6.4: Time domain variation of gyroscope error.

the order of one decade. This result is indicative of the algorithm’s efficacy in mitigating noise and enhancing the precision of the system when subjected to harmonic perturbations. These findings offer compelling evidence of the algorithm’s robustness and constitute a significant advancement. The application of this type of compensator for non-harmonical movements shall be further evaluated.

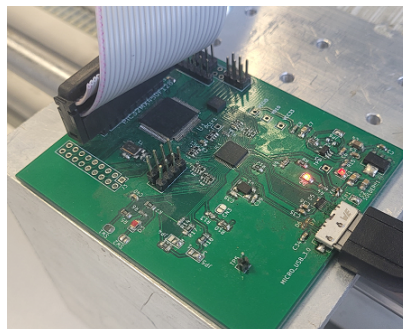


Figure 6.5: Experimental measurement HW.

6.3 Summary

The algorithms we have developed underwent an evaluation to assess their feasibility for real-time hardware implementation. Specifically, the non-linear least squares based algorithm was optimized to reduce computational load. By replacing nonlinear functions with precomputed values stored in look-up tables, we significantly reduced the computational power required. This optimization enables the algorithm to be effectively deployed on low-cost, real-time hardware without compromising precision. On the other hand, the deployment of an efficient artificial neural network based compensator presents substantial resource demands. Consequently, its implementation on either a microcontroller or an FPGA is economically infeasible when contrasted with the cost of low-cost MEMS gyroscopes. To practically assess the performance of these compensators, we utilized a dsPIC microcontroller as our target hardware in Figure 6.5. The microcontroller was programmed using code automatically generated from the Matlab/Simulink toolchain. A detailed evaluation of the compensator’s performance has been discussed in the preceding chapter.

7 Conclusion

The following objectives were set for this work:

1. Analysis of the effect of linear accelerations and jerks on MEMS gyroscopic sensors and their quantification.
2. Design of new models for linear acceleration compensation.
3. Implementation of the proposed method on real-time HW and experimental measurements.

The objectives have been met, i.e., to analyze the effect of acceleration and jerk, to design compensation models, and to implement the selected model on RT HW. Despite the specific functionality of the compensator, the work has many indirect results that have been achieved contextually, which is evident from the range of published papers.

Objectives 1 and 2 are very closely related in terms of application. The motivation for their solution was both engineering and pedagogical practice, which was independently initiated by the development of an unstable education model in the Mechatronics laboratory at the Brno University of Technology and from the perspective of the development of unstable electromechanical, dynamic systems requiring inertial sensors in cooperation with Hochschule Esslingen. The actual work carried out is described in Chapters 4, 5, and 6, while an introduction to the subject can be found in the research section 2. The first two objectives were met, but the applicability in practice is limited to the disturbance coming from harmonic signals and the delay associated with the dominant frequency extraction from discrete-time fast Fourier transformation. Still, this method can be considered as a founding stone and can be extended further or optimized. Objective 3 (Implementation of the proposed method on real-time HW and experimental measurements) proved to be more powerful than originally intended and with the potential for wider application beyond the field of gyroscopic sensors. Automatic code generation during the time of realization of this work has significantly advanced and proved to be a reliable workflow suitable not only for research purposes but also as a reliable industrial tool.

7.1 Thesis achievements

1. Based on the dynamic analysis, experimental methods were developed to evaluate the effect of linear accelerations and jerks on MEMS gyroscopic sensors. The evaluation includes an algorithm based on non-linear least squares, which makes it possible to quantify the aforementioned influence in an exact way. Using the data thus obtained, it is possible to unambiguously compare all types of MEMS gyroscopic sensors based on the criterion of sensitivity to acceleration and jerk disturbances. The results are described in Chapter 4. The initial part of this method was published at [3].

7 CONCLUSION

2. The algorithm derived from the non-linear least square method has been simplified to create a parametric compensation model of a single-mass MEMS gyroscopic sensor with an emphasis on low computational requirements. This model can be applied on a microcontroller. As a result, it is possible to cost-optimize the computational HW and achieve a reduction of error in standard deviation by 10 times relative to the measurement without a compensator. This model is described in Section 6.2. This result was presented at the Mechatronics 2019, an international conference held in Warsaw, Poland [4], and cited in [8].
3. Development and validation of a non-linear compensation model based on an artificial neural network. Compared to the previous parametric model, this is a more computationally demanding model. Based on the results from our work [3], this type of compensator achieved a reduction of error standard deviation by 4 times relative to the measurement without a compensator. This model is described in section 5.2. The result was published at [3].

7.2 Further research possibilities

The method presented here to quantify the effect of linear acceleration on a gyroscopic sensor was defined with the intention of using it in the widest possible range of applications. However, its functionality was tested on sets of harmonic signals and an extension to more general random noise would be beneficial. In the literature [9], [10], or [11] we often come across the issue of the influence of constant normal and tangential acceleration. We consider it beneficial to develop and test the methodology and compensation algorithms for the case of varying rotational accelerations (or non-constant normal and tangential acceleration).

The proposed compensation algorithms have rather specific functionality directly aiming at application in the single-axis two-wheel self-balancing personal transporter. It would be advisable to focus on the generalization of each method in more detail. In the analysis of the individual gyroscopic sensors, we observed frequencies where the sensitivity to external excitation deviated significantly from the general trend, explicitly around 3.5 Hz . We suspect that these may be harmonics of the resonant frequency associated with the internal mechanical structures of the MEMS gyroscope. We recommend further investigation of this occurrence, incorporating the insights into an enhanced compensator.

References

- [1] MAJID DADAFSHAR. APPLICATION NOTE 5830. *APPLICATION NOTE 5830*. 2014. Available also from: <http://www.maximintegrated.com/en/an5830>.
- [2] ACAR, Cenk; SHKEL, Andrei. MEMS Vibratory Gyroscopes. 2009. ISBN 978-0-387-09535-6. Available from DOI: 10.1007/978-0-387-09536-3.
- [3] SPACIL, T.; RAJCHL, M. Compensation of Linear Acceleration in Single-Mass MEMS Gyroscope. *Proceedings of the 2018 18th International Conference on Mechatronics - Mechatronika, ME 2018*. 2019, pp. 1–6. ISBN 9788021455443.
- [4] SPACIL, T.; RAJCHL, M.; BASTL, M.; NAJMAN, J.; APPEL, M. *Advances in Intelligent Systems and Computing*. Vol. 1044, Design of deterministic model for compensation of acceleration sensitivity in MEMS gyroscope. 2020. ISBN 9783030299927. ISSN 21945365. Available from DOI: 10.1007/978-3-030-29993-4{_}35.
- [5] *MPU-6050 — TDK InvenSense*. [N.d.]. Available also from: <https://invensense.tdk.com/products/motion-tracking/6-axis/mpu-6050/>.
- [6] *L3G4IS - MEMS motion sensor: three-axis digital output gyroscope for gaming and OIS - STMicroelectronics*. [N.d.]. Available also from: <https://www.st.com/en/mems-and-sensors/l3g4is.html#documentation>.
- [7] *SCC2000 Series Combined Gyro Sensor and Accelerometer — Gyro Sensors — Murata Manufacturing Co., Ltd.* [N.d.]. Available also from: <https://www.murata.com/en-global/products/sensor/gyro/overview/lineup/scc2000>.
- [8] INDEITSEV, D. A.; BELYAEV, Ya V.; LUKIN, A. V.; POPOV, I. A.; IGUMNOVA, V. S.; MOZHGOVA, N. V. Analysis of imperfections sensitivity and vibration immunity of MEMS vibrating wheel gyroscope. *Nonlinear Dynamics*. 2021, vol. 105, no. 2, pp. 1273–1296. ISSN 1573269X. Available from DOI: 10.1007/S11071-021-06664-0.
- [9] SAUKOSKI, Mikko; AALTONEN, Lasse; HALONEN, Kari A.I. Zero-rate output and quadrature compensation in vibratory MEMS gyroscopes. *IEEE Sensors Journal*. 2007. ISBN 1530-437X. ISSN 1530437X. Available from DOI: 10.1109/JSEN.2007.908921.
- [10] BANCROFT, Jared B.; LACHAPELLE, Gerard. Estimating MEMS gyroscope g-sensitivity errors in foot mounted navigation. In: *2012 Ubiquitous Positioning, Indoor Navigation, and Location Based Service, UPINLBS 2012*. 2012. ISBN 9781467319096. Available from DOI: 10.1109/UPINLBS.2012.6409753.
- [11] FAN, Chen; HU, Xiaoping; HE, Xiaofeng; TANG, Kanghua; LUO, Bing. Observability analysis of a MEMS INS/GPS integration system with gyroscope G-sensitivity errors. *Sensors (Switzerland)*. 2014. ISBN 8673184576. ISSN 14248220. Available from DOI: 10.3390/s140916003.

Curriculum Vitae

Personal Information:

Name: Ing. Tomáš Spáčil
Date of Birth: 13.12.1990
Citizenship: CZ
Email: tomas.spacil1@vutbr.cz

Education

2003 - 2010 Komenský Grammar School Vyškov
2010 - 2015 Bc. and Ing., Mechatronics, FME Brno University of Technology
2015 - 2023 Ph.D., Engineering Mechanics, FME Brno University of Technology

Employment

2015 Hochschule Esslingen - University of Applied Sciences, Research Scientist
2015 - 2020 FME Brno University of Technology, assistant
2016 - 2020 Mechsoft s.r.o., R&D engineer
2020 Czechoslovak Ocean Shipping Group, Antarctic Station Technician
2021 - to date Masaryk University Brno, Technical Manager of Czech Antarctica Stations
2021 - to date Thermo Fisher Scientific, R&D System Engineer

Language competence

Czech native
English fluent (C2)
Spanish basic (B1)

Technical competence & skills

Programming - Matlab, Python, LabView.
Signal processing, PCB design and testing, laboratory equipment, sensors.

Abstract

This Doctoral thesis deals with the development of a new type of forward compensator, specifically designed to counteract the effect of linear acceleration and jerk acting on MEMS gyro sensors. From the principle of inertial sensor function, additional undesirable forces (normal and tangential) occur when the gyro sensor is placed off the axis of rotation, which negatively affect the measurement of the desired angular velocity. However, the presence of these forces can be measured by an independent sensor, the accelerometer, and the output value of the gyro sensor can be compensated for in a suitable way, thus refining the indirectly measured value of the angular velocity. In the first part of the paper we identify the effect of the mentioned accelerations on MEMS gyroscopes, in the second part of the paper we design and test different compensators, evaluate their effectiveness and in the third part we implement a suitable algorithm on RT HW.

Abstrakt

Tato Disertační práce se zabývá vývojem nového typu dopředného kompenzátoru, speciálně určeného k potlačení vlivu lineárního zrychlení a ryvu působícího na MEMS gyroskopické senzory. Z principu funkce inerciálního snímače, dochází při umístění gyroskopického senzoru mimo osu rotace k vzniku dalších nežádoucích sil (normálové a tečné), které negativně ovlivňují měření žádané úhlové rychlosti. Přítomnost těchto sil je však možno měřit nezávislým senzorem, akcelerometrem, a vhodným způsobem kompenzovat výstupní hodnotu gyroskopického senzoru a tím zpřesnit nepřímo měřenou hodnotu úhlové rychlosti. V první části práce identifikujeme vliv zmíněných zrychlení na MEMS gyroskopy, v druhé části práce pak navrheme a otestujeme různé kompenzátory, vyhodnotíme jejich efektivitu a v třetí části vhodný algoritmus implementujeme na RT HW.